International Journal of Numerical Methods for Heat & Fluid Flow

Dispersion and damping characteristics of Rayleigh-type waves in KG nonlocal fractional piezo-thermo-electric semiconductor medium

Mohammed Aldandani
Mathematics Department, College of Science, Jouf University, Sakaka, Saudi Arabia

Soumik Das
School of Physical Sciences, Amrita Vishwa Vidyapeetham, Mysuru, India

Arun Kumar Yadav
School of Basic and Applied Sciences, K. R. Mangalam University, Gurugram, India

Murat Yaylacı
Department of Civil Engineering, Recep Tayyip Erdogan University, Rize, Türkiye, and

Vipin Gupta
Department of Mathematics, Gurugram University, Gurugram, India

Received 23 November 2025
Revised 14 February 2026
Accepted 20 February 2026

Abstract

Purpose – This study aims to investigate Rayleigh-type surface wave propagation in a piezo-thermo-electric semiconductor medium. Klein–Gordon-type nonlocal effects and a higher-order fractional three-phase-lag heat-conduction model are incorporated. The analysis examines how nonlocal elasticity, piezoelectric semiconducting behavior and advanced heat-conduction influence wave dispersion and attenuation.

Design/methodology/approach – Analytical solutions are obtained using the wave-mode method. The Durand–Kerner algorithm is applied to solve the characteristic equation and identify physically admissible surface wave modes. The analysis is performed for a half-space under isothermal and electrically insulated boundary conditions. Fractional derivatives and multiple phase lags are included to account for advanced thermal transport effects.

Findings – Numerical results show the variation in dispersion relations, phase velocity and attenuation with changes in spatial and temporal nonlocal parameters as well as phase lags. Surface particle trajectories are also evaluated. Sensitivity analysis highlights the distinct influence of higher-order thermal lags and nonlocal effects on wave propagation and energy dissipation.

Research limitations/implications – This investigation addresses a key gap in the literature by simultaneously incorporating Klein–Gordon nonlocality, fractional effects, thermo-electro-mechanical coupling and three-phase lag behavior in semiconductor media. The study also presents several limiting and

Funding: This work was funded by the Deanship of Graduate Studies and Scientific Research at Jouf University under grant No. DGSSR-2025-FC-01066.

Disclosure statement: The authors affirm that no financial, commercial or personal relationships exist that could be construed as a potential conflict of interest in this research.

International Journal of Numerical Methods for Heat & Fluid Flow

0961-5539
DOI 10.1108/HFF-11-2025-0930

special cases. These results provide a basis for future work on coupled wave phenomena in advanced functional materials with microstructural effects.

Practical implications – The outcomes support the development of smart surface devices, acoustic sensors and energy harvesting systems. The findings are relevant to applications in microelectronics, optoelectronics and seismic engineering.

Originality/value – This paper develops a framework for Rayleigh wave analysis in piezo-semiconductor media with Klein–Gordon-type nonlocal elasticity and a higher-order fractional three-phase-lag thermal model.

Keywords Piezo-semiconductor, SDG7, Klein–Gordon nonlocal elasticity, Rayleigh surface waves, Three-phase-lag model, Fractional derivative, Higher-order heat conduction

Paper type Research paper

Nomenclature

e_{ij} = component of strain;
τ^{*} = photo-generated carrier lifetime;
κ = thermal activation coupling parameter;
D_i = electric displacement;
φ = electrical potential;
C_E = specific heat at constant strain;
D_{ij}^{E} = carrier diffusion tensor;
θ = thermal temperature;
K_{ij} = components of the thermal conductivity;
α^{*} = relaxation parameter;
δ_{ij}^{N} = electronic deformation tensor;
η_{ijr}, ε_{ij} = piezo-thermal moduli tensors;
τ_v = phase lag of thermal disp. gradient;
c_{ijrl} = elastic stiffness tensor;
K_{ij} = components of thermal conductivity;
τ = temporal nonlocality parameter;
E_g = energy gap;
τ_i = pyroelectric constants;
τ_T = phase lag of the temperature gradient;
q_i^{*} = component of heat flux;
α = fractional-order parameter;
N = carrier density;
σ_{ij} = components of the nonlocal stress;
E_i = electric field density;
D_α = fractional-order operator;
ξ = spatial nonlocality parameter;
S^{*} = entropy;
τ_q = phase lag of heat flux;
ρ = density;
β_{ij}^{T} = thermal moduli tensors; and
K_{ij}^{*} = components of the rate of thermal conductivity.

1. Introduction

Semiconductors occupy an important position among engineering materials, lying between conductors and insulators in their electrical behavior. Their unique properties make them

essential in modern renewable energy technologies, especially in photovoltaic and solar energy systems (Neamen, 1992).

During the early decades of the 20th century, significant efforts were made to understand wave propagation in elastic solids. Many classical theories, however, assumed that thermal and mechanical disturbances travel at infinite speeds, which is physically unrealistic. To resolve this limitation, Biot (1956) introduced the coupled thermoelasticity framework based on Fourier's law of heat conduction, offering a more realistic description of thermo-mechanical interactions. Later, relaxation times were incorporated into the governing equations of motion and heat transfer (Lord and Shulman, 1967; Green and Lindsay, 1972), removing the assumption of instantaneous propagation. These developments led to the generalized theory of thermoelasticity, extending its applicability to a wide range of materials and physical processes (Chandrasekharaiah, 1986; Chandrasekharaiah, 1998). A notable advancement was made by Green and Naghdi (Green and Naghdi, 1991; Green and Naghdi, 1993; Green and Naghdi, 1992), who developed thermoelastic models known as Type II and Type III to describe energy dissipation in deformable solids. Their formulations offered deeper insight into wave propagation and energy transport in elastic media. Tzou (1995) later proposed the dual-phase-lag (DPL) model by introducing separate lag times for heat flux and temperature gradient to capture microscale heat transfer effects. Building on this, Roy Choudhuri (Choudhuri, 2007) introduced the three-phase-lag (TPL) model by incorporating an additional lag in the thermal displacement gradient, improving the modeling of microscale heat conduction.

The foundational work of Edelen and Laws (1971) established the basis of nonlocal interaction theory. Building on this, Eringen and Edelen (1972) incorporated global balance laws and thermodynamic principles to develop a framework for nonlocal elasticity in continua. Research on wave propagation in nonlocal thermoelastic media has since grown significantly (Biswas, 2020; Saeed and Abbas, 2022; Zhang *et al.*, 2014). However, Eringen's differential model has been critically examined, with studies by Romano *et al.* (2017) and Kaplunov *et al.* (2022) and Kaplunov *et al.* (2023) pointing out certain inconsistencies through counterexamples. To address these issues, Anh and Vinh (2023) proposed a weakly nonlocal elasticity formulation and studied surface waves at the interface of two such media. This work was later extended by Anh *et al.* (2023) to Rayleigh-type waves under impedance boundary conditions. Further progress was made by Lazar and Agiasofitou (2022), who developed a Klein–Gordon-based weakly nonlocal elasticity model introducing both characteristic length and time scales, thereby incorporating temporal nonlocal effects.

The scientific community has shown growing fascination with piezoelectric semiconductors, recognizing their immense potential and multifaceted applications (Smith, 2005). The intricate coupling between electrical, thermal and mechanical responses presents exciting opportunities for innovation across diverse technological domains. The theoretical groundwork for understanding such interactions was first laid by Mindlin (1974), who formulated the fundamental equations describing temperature–piezoelectric coupling. Building upon this framework, Chandrasekharaiah (1988) advanced the field by integrating the concept of finite wave velocity into thermo-piezoelectric analysis. A major conceptual refinement was later contributed by Aouadi (2006), who developed a generalized thermoelasticity model specifically adapted for piezoelectric materials exhibiting temperature-dependent properties. Lotfy and his collaborators (Lotfy and El-Bary, 2022; Lotfy *et al.*, 2020; Lotfy *et al.*, 2021) conducted extensive investigations into magneto-thermo-elastic responses and microtemperature phenomena in semiconductor materials. Mahdy and his collaborators (Adel *et al.*, 2025; Ailawalia *et al.*, 2025; Mahdy *et al.*, 2026)

examined fractional stability analysis, thermal shock in semiconductors and nonlocal photoacoustic wave propagation, emphasizing the impact of memory and nonlocal interactions. Chen *et al.* (2024) used piezoelectric ultrasonic resonance techniques to evaluate pretension stress in small-sized bolts. Their results demonstrated the effectiveness of wave-based resonance signatures for structural stress assessment. He *et al.* (2025) investigated mechanical stress wave detection in power semiconductor devices using bare FBG sensors.

Fractional calculus has gained increasing importance in recent years and is widely used across fields such as control theory, signal processing and electromagnetic modeling. The concept dates back to 1695, when de L'Hospital first raised the question of derivatives of noninteger order. As noted by Diethelm and Ford (2002), the idea emerged from viewing differentiation as the inverse of integration. Among various definitions (de Oliveira and Tenreiro Machado, 2014), the Caputo and Riemann–Liouville forms are most commonly used due to their strong nonlocal features (Wang and Li, 2021). Abouelregal and collaborators (Abouelregal, 2020a, 2020b; Abouelregal *et al.*, 2021a, 2021b; Abouelregal *et al.*, 2021a, 2021b) extended heat-conduction theories using higher-order time derivatives, improving the modeling of thermal lag at micro and nanoscale levels. Lewis and co-researchers (Lewis and Garner, 1972; Lewis *et al.*, 1997; Lewis *et al.*, 2004; Lewis *et al.*, 2004; Lewis *et al.*, 1991) developed finite-element formulations for coupled heat transfer and fluid flow. Further studies on fractional, two-temperature and nonlocal thermoelastic wave propagation have been reported in Pathania *et al.* (2022), Yadav *et al.* (2022), Abouelregal *et al.* (2022) and Pathania *et al.* (2023). Energy interactions in piezo-thermo-electric media were later examined by Gupta and his team (Gupta *et al.*, 2023; Barak *et al.*, 2023; Gupta and Barak, 2023a, 2023b).

The present investigation develops a generalized theoretical framework to analyze Rayleigh-type surface wave propagation in a piezo-thermo-electric semiconductor medium by incorporating Klein–Gordon-type spatio-temporal nonlocal elasticity together with a higher-order fractional TPL heat-conduction model. The formulation simultaneously accounts for thermo-mechanical deformation, electric potential, carrier density transport and advanced heat transfer mechanisms within a unified multi-physics setting. The novelty of the work lies in the integration of Klein–Gordon nonlocal interaction with fractional thermal memory and semiconductor plasma effects, which, to the best of the authors' knowledge, has not been reported in the context of Rayleigh surface wave analysis. The model further enables evaluation of dispersion behavior, attenuation characteristics and particle motion under the combined influence of spatial nonlocality, temporal memory and higher-order thermal lags. The outcomes of this study are expected to contribute toward the design and optimization of surface acoustic wave devices, piezoelectric semiconductor sensors, thermal energy harvesters and micro-nano electromechanical systems, where coupled thermo-electro-mechanical wave dynamics play a critical operational role.

2. Fundamental equations

Consider an infinite elastic continuum occupying a domain V, influenced by body forces F_i. The linear momentum balance governing the system can be expressed as:

$$\sigma_{ij,j}(\mathrm{x},t) + F_i(\mathrm{x},t) = \rho \ddot{u}_i(\mathrm{x},t), \tag{1}$$

where u_i the displacement field, σ_{ij} is the nonlocal stress and ρ represents the mass density of the medium:

- Nonlocal constitutive relations

In a spatio–temporal nonlocal formulation, the constitutive relationship is described through a convolution integral of the stress and strain fields (Lazar and Agiasofitou, 2022; Agiasofitou and Lazar, 2023):

$$\sigma_{ij}(\mathrm{x},t) = \int_{-\infty}^{t}\int_{V} C_{ijkl}(\mathrm{x},t;x',t')\,e_{kl}(x't')dV'dt', \tag{2}$$

where C_{ijkl} is a fourth-order tensor that defines the nonlocal elastic moduli, while $e_{kl} = \frac{1}{2}(u_{k,l} + u_{l,k})$ denotes the infinitesimal strain tensor, $\mathrm{x}, \mathrm{x}' \in V \subseteq \Re^3$.

Substituting the above relation into the equilibrium condition (1) gives the integral representation of motion for nonlocal elastic continua:

$$\frac{\partial}{\partial x_j}\int_{-\infty}^{t}\int_{V} C_{ijkl}(\mathrm{x},\mathrm{t};x't')\,e_{kl}(x',t')dV'dt' + F_i(\mathrm{x},t) = \rho\ddot{u}_i(\mathrm{x},t). \tag{3}$$

The tensor C_{ijkl} (x-x$'$, $t - t'$) may be decoupled into the product of a scalar attenuation kernel α(x-x$'$, $t - t'$) and a local elastic modulus tensor C^L_{ijkl}, i.e.:

$$C_{ijkl}(\mathrm{x}-x't-t') = C^L_{ijkl}\,\alpha(\mathrm{x}-x',t-t'). \tag{4}$$

This kernel represents the degree of spatial and temporal interaction across material points.

With this substitution, the nonlocal stress becomes a space–time convolution of the attenuation kernel with the classical Cauchy stress tensor σ^L_{ij}:

$$\sigma_{ij}(\mathrm{x},t) = \int_{-\infty}^{t}\int_{V} C_{ijkl}(\mathrm{x},t;x',t')\,e_{kl}(x',t')dV'dt' = \alpha(\mathrm{x},t)*\sigma^L_{ij}(\mathrm{x},t),$$

where "*" indicates convolution over both position and time domains.

For homogeneous isotropic media, the stress–strain relation may be written as:

$$\sigma_{ij}(\mathrm{x},t) = \int_{-\infty}^{t}\int_{V} \alpha(|\mathrm{x}-x',t-t'|)\sigma^L_{ij}(x',t')dV'dt', \tag{5}$$

where $\sigma^L_{ij} = \lambda e_{kk}\delta_{ij} + 2\mu e_{ij}$, λ and μ being the Lamé constants.

The kernel function α acts as a transfer function capturing the long-range mechanical interaction. From a mathematical viewpoint, this kernel can be identified as a Green's function associated with a linear differential operator L.

For unbounded media, the operator is typically expressed in the form:

$$L\alpha(|\mathrm{x}-x't-t'|) = \delta(\mathrm{x}-x')\delta(t-t'), \tag{6}$$

where $\delta(\bullet)$ is the Dirac delta function.

Applying L to equation (5) and invoking equation (6) yields a differential representation of the nonlocal constitutive law:

$$L\sigma_{ij} = \sigma_{ij}^{L}. \tag{7}$$

Here, σ_{ij}^{L} represents the source term that recovers the classical local response when nonlocality vanishes.

Consequently, the scalar kernel α serves as the Green's function for operator L, enabling the equivalence between the integral and differential descriptions of nonlocal elasticity.

Assuming that L, is a linear operator with constant coefficients, the equation of motion follows directly by combining equations (1) and (7):

$$L\left(\rho\, \partial_t^2 u_i\right) - \partial_j \sigma_{ij}^{L} = LF_i. \tag{8}$$

• Klein–Gordon-type nonlocal operator formulation

The operator L, is frequently approximated through a Helmholtz-type relation, which in a dynamic setting transforms into a hyperbolic differential operator of the form (Lazar and Agiasofitou, 2022; Agiasofitou and Lazar, 2023):

$$L \equiv 1 - \xi^2 \nabla^2 + \tau^2 \frac{\partial^2}{\partial t^2}. \tag{9}$$

Here, ∇^2 is the Laplacian, ξ defines the intrinsic material length scale linked to spatial nonlocality and $\tau \in \mathbb{R}^+$ represents the characteristic time scale related to temporal interactions. The parameter $\xi = e_0 a_{cl}$ corresponds to a microstructural measure where e_0 is material coefficient. Defining a nonlocal propagation speed $c \in \mathbb{R}^+$ as $c = \xi/\tau$, the operator L, assumes the form of a Klein–Gordon-type (KG) operator. Following Eringen (1983), the identification $\xi \simeq 0.39a$, where a denote the lattice constant, offers a physically consistent estimate of the spatial characteristic length inherent in atomic lattices:

• *Constitutive relations* (Gupta *et al.*, 2024; Iovane and Nasedkin, 2010):

$$\left(1 - \xi^2 \nabla^2 + \tau^2 \frac{\partial^2}{\partial t^2}\right)\sigma_{ij} = \sigma_{ij}^{L} = c_{ijkl} e_{kl} - \eta_{ijk} E_k - \beta_{ij}^{T} \theta - \delta_{ij}^{N} N, \tag{10}$$

$$\left(1 - \xi^2 \nabla^2 + \tau^2 \frac{\partial^2}{\partial t^2}\right) D_i = D_i^{L} = \eta_{ijk} e_{jk} + \varepsilon_{ij} E_j + \tau_i \theta, \tag{11}$$

$$\left(1 - \xi^2 \nabla^2 + \tau^2 \frac{\partial^2}{\partial t^2}\right)\rho S^{*} = \left(\rho S^{*}\right)^{L} = \beta_{ij}^{T} e_{ij} + \tau_i E_i + \frac{\rho C_E \theta}{\theta_0}. \tag{12}$$

• *Equations of motion:*

$$\sigma_{ij,j}^{L} + \left(1 - \xi^2 \nabla^2 + \tau^2 \frac{\partial^2}{\partial t^2}\right) F_i = \rho \left(1 - \xi^2 \nabla^2 + \tau^2 \frac{\partial^2}{\partial t^2}\right) \ddot{u}_i, \tag{13}$$

$$D_{i,i} = 0, \quad \text{where} \quad E_i = -\varphi_{,i}, \tag{14}$$

• *Energy scale equation:*

$$\rho\theta_0 S^* = -q^*_{i,i}. \tag{15}$$

• *Nonlocal higher order fractional TPL heat transfer law* (Abouelregal, 2020a, 2020b):

$$\left(1-\xi^2\nabla^2+\tau^2\frac{\partial^2}{\partial t^2}\right)\left(1+\sum_{m=1}^{n}\frac{\tau_q^{m\alpha}}{\Gamma(m\alpha+1)}\frac{\partial^{m\alpha}}{\partial t^{m\alpha}}\right)q_i^* = -K_{ij}\frac{\partial}{\partial t}\left(1+\sum_{m=1}^{p}\frac{\tau_T^{m\alpha}}{\Gamma(m\alpha+1)}\frac{\partial^{m\alpha}}{\partial t^{m\alpha}}\right)\theta_{,i} - \int\frac{E_g\dot{N}}{\tau^*}dx_i - K_{ij}^*\left(1+\sum\nolimits_{m=1}^{l}\frac{\tau_v^{m\alpha}}{\Gamma(m\alpha+1)}\frac{\partial^{m\alpha}}{\partial t^{m\alpha}}\right)\theta_{,i} \tag{16}$$

• *Nonlocal higher order fractional TPL heat model*
Using equations (12), (15) and (16), we obtain:

$$K_{ij}\frac{\partial}{\partial t}\left(1+\sum_{m=1}^{p}\frac{\tau_T^{m\alpha}}{\Gamma(m\alpha+1)}\frac{\partial^{m\alpha}}{\partial t^{m\alpha}}\right)\theta_{,ij}+K_{ij}^*\left(1+\sum_{m=1}^{l}\frac{\tau_v^{m\alpha}}{\Gamma(m\alpha+1)}\frac{\partial^{m\alpha}}{\partial t^{m\alpha}}\right)\theta_{,ij} + E_g\frac{N}{\tau^*} = \left(1+\sum_{m=1}^{n}\frac{\tau_q^{m\alpha}}{\Gamma(m\alpha+1)}\frac{\partial^{m\alpha}}{\partial t^{m\alpha}}\right)\left(\rho C_E\ddot{\theta}+\theta_0\left(\beta_{ij}^T\ddot{u}_{i,j}-\tau_i\ddot{\varphi}_{,i}\right)\right) \tag{17}$$

• *Thermo-plasma transport equation:*

$$\frac{\partial N}{\partial t} = D_{ij}^E N_{,ij} - \frac{N}{\tau^*} + \kappa\theta \tag{18}$$

where $i, j, k, l = 1, 2, 3$ and the higher orders $p, l, n \in \mathrm{N}$. The σ_{ij}^L, $\left(\sigma_i^1\right)^L$, D_i^L and $(\rho S^*)^L$ are linked with local thermal piezoelectric medium, and α is the fractional-order parameter and $\Gamma(.)$ is the gamma function.

2.1 Limiting cases

The higher-order fractional TPL model can be converted into another form of heat-conduction model under particular limiting conditions when:

- If $\tau_q = \tau_v = \tau_T = 0$ and $K_{ij}^* = 0$ then corresponds to Biot model (Biot, 1956).
- If $n = 1$, $\tau_q > 0$, $\tau_T = \tau_v = 0$, $K_{ij}^* = 0$ and $\alpha = 1$ then LS model (Lord and Shulman, 1967).
- If $n = 2$, $p = 1$, $K_{ij}^* = \tau_v = 0$ and $\alpha = 1$ then DPL model (Tzou, 1995).
- If $n = 2$, $p = l = 1$ and $\alpha = 1$ corresponds to TPL model (Choudhuri, 2007).

2.2 Physical interpretation of model parameters

For clearer physical insight into the proposed theoretical formulation, it is useful to interpret the principal nonlocal, thermal and fractional parameters in terms of measurable microstructural and transport mechanisms. The spatial nonlocal parameter ξ represents an intrinsic material length scale that characterizes the range of long-distance interatomic interactions. Physically, it is associated with lattice spacing, grain size and microstructural heterogeneity. Larger values of ξ indicate stronger nonlocal coupling, meaning that the stress state at a point is influenced by the deformation of surrounding material points over a finite distance. Such behavior becomes prominent in nano-structured and fine-grained semiconductor media. The thermal relaxation time τ corresponds to the phonon relaxation process within the medium. It denotes the finite time required for heat carriers to restore

thermal equilibrium after a disturbance. In generalized thermoelasticity, this parameter governs the transition from diffusive to wave-type heat transport and reflects phonon scattering, collision frequency and thermal inertia effects. The fractional-order parameter α describes the degree of thermal memory present in the system. When $\alpha = 1$, the model reduces to classical integer-order heat conduction. However, for $\alpha < 1$, the heat transport process becomes history-dependent, indicating hereditary energy transfer. This fractional behavior captures anomalous diffusion and long-memory effects that are commonly observed in complex semiconductor and microstructured thermoelastic materials. These interpretations establish a direct connection between the mathematical parameters and the underlying physical processes governing wave dispersion and damping in the proposed nonlocal fractional thermo-piezoelectric semiconductor framework.

3. Formulation of the problem

In this study, we analyze the propagation of Rayleigh-type surface waves in a semi-infinite piezoelectric semiconductor medium modeled within the framework of Klein–Gordon nonlocal elasticity and advanced fractional thermal dynamics:

• Geometrical configuration and wave assumptions

A Cartesian coordinate system is adopted for geometrical description, with the wave propagation axis aligned along the x-direction and the positive z-axis directed into the bulk of the medium. Figure 1 illustrates the setup for the semi-infinite domain. The surface waves motion is confined to the xz –plane, involving coupled variations in displacement $\overrightarrow{u} = (u(x, z, t), 0, w(x, z, t))$, electric potential $\varphi = \varphi(x, z, t)$, carrier density $N = N(x, z, t)$ and temperature $\theta = \theta(x, z, t)$.

• Constitutive relations in nonlocal framework

As a consequence, the constitutive relations for stress and strain, together with the laws governing electric displacement, originally formulated in equations (10) and (11), are now reformulated within the present KG nonlocal framework as follows:

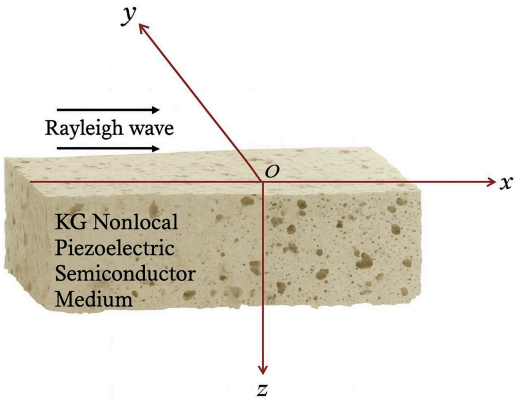

Figure 1: Schematic layout of the problem
Source: Created by the authors

$$\left(1-\xi^2\nabla^2+\tau^2\frac{\partial^2}{\partial t^2}\right)\sigma_{xx}=\sigma_{xx}^L=\eta_{31}\varphi_{,z}-\delta_1^N N-\beta_1^T\theta+c_{11}u_{,x}+c_{13}w_{,z}, \tag{19}$$

$$\left(1-\xi^2\nabla^2+\tau^2\frac{\partial^2}{\partial t^2}\right)\sigma_{xz}=\sigma_{xz}^L=\eta_{15}\varphi_{,x}+c_{55}(u_{,z}+w_{,x}), \tag{20}$$

$$\left(1-\xi^2\nabla^2+\tau^2\frac{\partial^2}{\partial t^2}\right)\sigma_{zz}=\sigma_{zz}^L=\eta_{33}\varphi_{,z}-\delta_3^N N-\beta_3^T\theta+c_{13}u_{,x}+c_{33}w_{,z}, \tag{21}$$

$$\left(1-\xi^2\nabla^2+\tau^2\frac{\partial^2}{\partial t^2}\right)D_x=D_x^L=-\varepsilon_{11}\varphi_{,x}\eta_{15}\left(u_{,z}+w_{,x}\right), \tag{22}$$

$$\left(1-\xi^2\nabla^2+\tau^2\frac{\partial^2}{\partial t^2}\right)D_z=D_z^L=-\varepsilon_{33}\varphi_{,z}+\tau_3\theta+\eta_{31}u_{,x}+\eta_{33}w_{,z}, \tag{23}$$

where:

$$\nabla^2=\frac{\partial^2}{\partial x^2}+\frac{\partial^2}{\partial z^2}.$$

• Reduced field equations

Incorporating equations (19) and (20), the motion equations (13) and (14), ignoring body forces, can be expressed as:

$$c_{11}\frac{\partial^2 u}{\partial x^2}+c_{55}\frac{\partial^2 u}{\partial z^2}+(c_{13}+c_{55})\frac{\partial^2 w}{\partial x\partial z}-\beta_1^T\frac{\partial\theta}{\partial x}-\delta_1^N\frac{\partial N}{\partial x}+(\eta_{31}+\eta_{15})\frac{\partial^2\varphi}{\partial x\partial z}=\rho\left(1-\xi^2\nabla^2+\tau^2\frac{\partial^2}{\partial t^2}\right)\frac{\partial^2 u}{\partial t^2}, \tag{24}$$

$$c_{55}\frac{\partial^2 w}{\partial x^2}+c_{33}\frac{\partial^2 w}{\partial z^2}+(c_{13}+c_{55})\frac{\partial^2 u}{\partial x\partial z}-\beta_3^T\frac{\partial\theta}{\partial z}-\delta_3^N\frac{\partial N}{\partial z}+\eta_{15}\frac{\partial^2\varphi}{\partial x^2}+\eta_{33}\frac{\partial^2\varphi}{\partial z^2}=\rho\left(1-\xi^2\nabla^2+\tau^2\frac{\partial^2}{\partial t^2}\right)\frac{\partial^2 w}{\partial t^2}, \tag{25}$$

$$\eta_{15}\frac{\partial^2 w}{\partial x^2}+\eta_{33}\frac{\partial^2 w}{\partial z^2}+(\eta_{31}+\eta_{15})\frac{\partial^2 u}{\partial x\partial z}-\varepsilon_{11}\frac{\partial^2\varphi}{\partial x^2}-\varepsilon_{33}\frac{\partial^2\varphi}{\partial z^2}+\tau_3\frac{\partial\theta}{\partial z}=0, \tag{26}$$

The transport equation for thermo-plasma in the *xz* –plane:

$$\frac{\partial N}{\partial t}=\left(D_1^E\frac{\partial^2 N}{\partial x^2}+D_3^E\frac{\partial^2 N}{\partial z^2}\right)-\frac{N}{\tau^*}+\kappa\theta. \tag{27}$$

Equation (17) leads to the reduced form of the higher-order TPL fractional heat equation in xz –plane as:

$$\left(1+\sum_{m=1}^{p}\frac{\tau_T^{m\alpha}}{\Gamma(m\alpha+1)}\frac{\partial^{m\alpha}}{\partial t^{m\alpha}}\right)(K_1\theta_{,xx}+K_3\theta_{,zz})+\left(1+\sum_{m=1}^{l}\frac{\tau_v^{m\alpha}}{\Gamma(m\alpha+1)}\frac{\partial^{m\alpha}}{\partial t^{m\alpha}}\right)(K_1^*\theta_{,xx}+K_3^*\theta_{,zz})$$
$$=-E_g\frac{\dot{N}}{\tau^*}+\left(1+\sum_{m=1}^{n}\frac{\tau_q^{m\alpha}}{\Gamma(m\alpha+1)}\frac{\partial^{m\alpha}}{\partial t^{m\alpha}}\right)\left(\rho C_E\ddot{\theta}+\theta_0(\beta_1\ddot{u}_{x,x}+\beta_3\ddot{u}_{z,z}-\tau_3\ddot{\varphi}_{,z})\right), \tag{28}$$

where, $K_{ij}=K_i\delta_{ij},\ \beta_{ij}^T=\beta_i^T\delta_{ij},\ K_{ij}^*=K_i^*\delta_{ij}$.

4. Solution of the problem

The fundamental solutions describing harmonic plane wave propagation in a thermo-piezoelectric semiconductor medium, with field amplitude $(\widetilde{u},\ \widetilde{w},\ \widetilde{\theta},\ \widetilde{\varphi},\ \widetilde{N})$ corresponding to each relevant variable (u, w, θ, φ, N), are given by:

$$(u,\ w,\ \theta,\ \varphi,\ N)=(\widetilde{u},\ \widetilde{w},\ \widetilde{\theta},\ \widetilde{\varphi},\ \widetilde{N})\exp[\iota\omega(qx+sz-t)], \tag{29}$$

where the associated slowness vectors are denoted by specified symbols q, s and ω represents the angular frequency.

Key transformation steps

The principal analytical transformations involved in the solution procedure may be summarized as follows:

- The coupled governing partial differential equations are formulated within the Klein–Gordon nonlocal and fractional thermo-piezoelectric semiconductor framework.
- Harmonic plane wave solutions are assumed for all field variables to convert the governing equations from the space–time domain into the frequency–wave number domain.
- Substitution of the harmonic expressions reduces the coupled differential equations to a system of homogeneous algebraic equations.
- The resulting system is arranged in matrix form, and the vanishing of the determinant yields the characteristic secular equation governing Rayleigh-type wave propagation.
- The complex roots of the dispersion equation are then evaluated numerically under radiation conditions to obtain admissible wave modes.

By substituting equation (29) into equations (24)–(28), we obtain the following set of homogeneous equations:

$$(g_{11}+g_{12}s^2)\widetilde{u}+(g_{13}s)\widetilde{w}-(g_{14})\widetilde{N}-(g_{15})\widetilde{\theta}+(g_{16}s)\widetilde{\varphi}=0, \tag{30}$$

$$(g_{21}s)\widetilde{u}+(g_{22}+g_{23}s^2)\widetilde{w}-(g_{24}s)\widetilde{N}-(g_{25}s)\widetilde{\theta}+(g_{26}+g_{27}s^2)\widetilde{\varphi}=0, \tag{31}$$

$$(g_{31})\widetilde{u}+(g_{32}s)\widetilde{w}+(g_{33})\widetilde{N}+(g_{34}+g_{35}s^2)\widetilde{\theta}-(g_{36})\widetilde{\varphi}=0, \tag{32}$$

$$(g_{41}s)\widetilde{u} + \left(g_{42} + g_{27}s^2\right)\widetilde{w} + (0)\widetilde{N} + (g_{43}s)\widetilde{\theta} - \left(g_{44} + g_{45}s^2\right)\widetilde{\varphi} = 0, \tag{33}$$

$$(0)\widetilde{u} + (0)\widetilde{w} + \left(g_{51} + g_{52}s^2\right)\widetilde{N} + (g_{53})\widetilde{\theta} + (0)\widetilde{\varphi} = 0, \tag{34}$$

where:

$$g_{11} = c_{11}q^2 - \rho(1 + \omega^2\xi^2q^2 - \tau^2\omega^2), \quad g_{12} = c_{55} - \rho\omega^2\xi^2, \quad g_{13} = (c_{13} + c_{55})q, \quad g_{14} = -\delta_1^N qb^{-1}$$

$$b = -\iota\omega, \quad g_{15} = -\beta_1^T qb^{-1}, \quad g_{16} = (\eta_{31} + \eta_{15})q, \quad g_{21} = (c_{13} + c_{55})q, \quad g_{22} = c_{55}q^2 - \rho(1 + \xi^2\omega^2q^2 - \tau^2\omega^2)$$

$$g_{23} = c_{33} - \rho\xi^2\omega^2, \quad g_{24} = -\delta_3^N b^{-1}, \quad g_{25} = -\beta_3^T b^{-1}, \quad g_{26} = \eta_{15}q^2, \quad g_{27} = \eta_{33}, \quad g_{31} = \theta_0\beta_1^T bq, \quad g_{32} = \theta_0\beta_3^T b$$

$$g_{33} = -E_g(\tau^* b)^{-1}, \; g_{34} = L_1K_1q^2b + L_2K_1^*q^2 - \rho C_E, \quad g_{35} = L_1K_3b + L_2K_3^*, \quad g_{36} = \theta_0\tau_3 b, \quad b = -\iota\omega$$

$$g_{41} = (\eta_{31} + \eta_{15})q, \quad g_{42} = \eta_{15}q^2, \quad g_{43} = \tau_3 b^{-1}, \quad g_{44} = \varepsilon_{11}q^2, \quad g_{45} = \varepsilon_{33}, \quad g_{51} = D_1^E q^2 - b^{-1} + \omega^{-2}(\tau^*)^{-1},$$

$$g_{52} = D_3^E, \quad g_{53} = \kappa b^{-2}.$$

$$L_1 = \frac{1 + \sum_{m=1}^{p} \dfrac{\tau_T^{m\alpha} t^{-m\alpha} E_{1,1-m\alpha}(b)}{\Gamma(m\alpha + 1)}}{1 + \sum_{m=1}^{n} \dfrac{\tau_q^{m\alpha} t^{-m\alpha} E_{1,1-m\alpha}(b)}{\Gamma(m\alpha + 1)}}, \quad L_2 = \frac{1 + \sum_{m=1}^{l} \dfrac{\tau_v^{m\alpha} t^{-m\alpha} E_{1,1-m\alpha}(b)}{\Gamma(m\alpha + 1)}}{1 + \sum_{m=1}^{n} \dfrac{\tau_q^{m\alpha} t^{-m\alpha} E_{1,1-m\alpha}(b)}{\Gamma(m\alpha + 1)}},$$

where $E_{\alpha_1,\alpha_2}(z)$ is the Mittag–Leffler function for any $z \in \mathbb{C}$ in two parameters α_1, $\alpha_2 \in \mathbb{C}$ with $\Re(\alpha_1) > 0$ defined as (Garrappa, 2015; Gorenflo and Mainardi, 2019):

$$E_{\alpha_1,\alpha_2}(z) = \sum_{k=0}^{\infty} \frac{z^k}{\Gamma(\alpha_1 k + \alpha_2)} \; .$$

The existence of nontrivial solutions for equations (30)–(34) is contingent upon the satisfaction of the associated characteristic equation:

$$\left(A_1 s^{10} + A_2 s^8 + A_3 s^6 + A_4 s^4 + A_5 s^2 + A_6\right)\left\{\widetilde{u},\ \widetilde{w},\ \widetilde{N},\ \widetilde{T},\ \widetilde{\varphi}\right\} = 0. \tag{35}$$

The coefficients A_i,$(i = 1 - 6)$ are determined through standard linear algebraic techniques involving the vanishing of the determinant. By applying the Durand–Kerner (Burden *et al.*, 2015) root-finding method to equation (35), ten pairs of complex conjugate roots are computed. The physically meaningful roots are subsequently selected according to the radiation conditions $\Im(s_n) > 0$ appropriate for a semi-infinite domain $z > 0$, ensuring that solutions represent decaying fields with increasing depth. Specifically, imposing that the real part of the root remains positive within the prescribed half-space ensures attenuation away from the boundary. As a result, the five distinct real parts of the retained roots s_p, $p = 1 - 5$ define unique slowness vectors $(q,\ s_p)$, each corresponding to a decaying wave mode in the semiconductor medium.

Consequently, the following presents the formal solution adhering to the radiation condition:

$$(u,\ w,\ N,\ \theta,\ \varphi) = \sum_{m=i}^{5} (1,\ P_m,\ Q_m,\ R_m,\ S_m)\widetilde{u}_m \exp[\iota\omega(qx + s_m z - t)]. \tag{36}$$

The value of amplitude ratios P_m, Q_m, R_m and S_m can be obtained by solving this system:

$$\begin{bmatrix} P_m \\ Q_m \\ R_m \\ S_m \end{bmatrix} = \begin{bmatrix} g_{13}s_m & -g_{14} & -g_{15} & g_{16}s_m \\ g_{22}+g_{23}s_m^2 & -g_{24}s_m & -g_{25}s_m & g_{26}+g_{27}s_m^2 \\ g_{32}s_m & g_{33} & g_{34}+g_{35}s_m^2 & -g_{36} \\ g_{42}+g_{27}s_m^2 & 0 & g_{43}s_m & -g_{44}-g_{45}s_m^2 \end{bmatrix}^{-1} \begin{bmatrix} -g_{11}-g_{12}s_m^2 \\ -g_{21}s_m \\ -g_{31} \\ -g_{41}s_m \end{bmatrix} \tag{37}$$

Using equation (36), (21), (22), (24) and (26) are recast in the following form:

$$(\sigma_{xz},\ \sigma_{zz},\ D_z) = \sum_{r=1}^{5} \iota\omega(\Upsilon_{1r},\ \Upsilon_{2r},\ \Upsilon_{3r})\tilde{u}_r \exp[\iota\omega(qx + s_r z - t)], \tag{38}$$

where:

$$\Upsilon_{1r} = \Upsilon_{1r}^L\left[1-\tau^2\omega^2-\xi^2\omega^2\left(q^2+s_r^2\right)\right], \quad \Upsilon_{2r} = \Upsilon_{2r}^L\left[1-\tau^2\omega^2-\xi^2\omega^2\left(q^2+s_r^2\right)\right],$$

$$\Upsilon_{3r} = \Upsilon_{4r}^L\left[1-\tau^2\omega^2-\xi^2\omega^2\left(q^2+s_r^2\right)\right], \quad \Upsilon_{1r}^L = c_{55}(s_r+qP_r)+\eta_{15}qS_r,$$

$$\Upsilon_{2r}^L = c_{13}q + c_{33}s_rP_r + \eta_{33}S_rs_r - \delta_3^N Q_r - \beta_3^T R_r,\ \Upsilon_{3r}^L = \eta_{31}q + \eta_{33}s_rP_r - \varepsilon_{33}s_rS_r + \tau_3 R_r$$

5. Boundary conditions

At the free surface $z = 0$ of the thermal piezoelectric semiconductor medium incorporating KG nonlocal effects, the following boundary conditions are imposed.

Mechanical conditions:

$$\sigma_{xz} = 0, \quad \sigma_{zz} = 0, \tag{39}$$

Electrical displacement condition:

$$D_z = 0, \tag{40}$$

Thermal condition:

$$\theta = 0, \tag{41}$$

Carrier density condition:

$$\frac{\partial N}{\partial z} = \frac{s_N N}{D_1^E}. \tag{42}$$

Meanwhile, as carriers diffuse through the medium, they penetrate the surface with a relatively low likelihood of recombination, attributable to the constant rate s_N at which recombination occurs.

6. Derivation of the secular equation

The Rayleigh-type surface waves secular equation is established by formulating the boundary value problem for the linearized field equations of the medium. From equations (36), (38) and (39)–(42), we derive a coupled system of equations in $\widetilde{u}_r$:

$$\sum_{r=1}^{5} \Upsilon_{pr}\widetilde{u}_r = 0, \ (p = 1-5) \tag{43}$$

where:

$$\Upsilon_{4r} = R_r, \quad \Upsilon_{5r} = \left(bs_r - s_N/D_1^E\right)Q_r.$$

A nontrivial solution is possible only when a specific condition is satisfied, namely, $\det\{\Upsilon_{5\times5}\} = 0$. This constraint results in the dispersion equation governing Rayleigh-type surface wave propagation in the chosen half-space. To determine the Rayleigh-type wave speed, the complex secular equation is evaluated numerically using the Newton–Raphson method, and the resulting complex root is denoted by c. The associated phase velocity varies with frequency, confirming that Rayleigh waves in the semiconductor medium exhibit dispersion. The imaginary part of c also reflects attenuation, where a positive value signifies exponential decay of the wave amplitude with penetration depth. The phase velocity and attenuation coefficient are subsequently computed using the classical expressions (Gupta *et al.*, 2024):

$$\text{Phase velocity} : V = \frac{|c^2|}{\Re(c)}. \tag{44}$$

$$\text{Attenuation coefficient} : Q^{-1} = \frac{\Im\left(1/c^2\right)}{\Re\left(1/c^2\right)}. \tag{45}$$

7. Path of the surface particle

The displacement expressions given by equation (36) are used to compute the path profile of surface particles in the medium, where c designates the Rayleigh-type wave motion. In this analysis, the mechanical displacement components are defined as:

$$(u, \ w) = \sum_{m=i}^{5} (1, \ P_m)\widetilde{u}_m \exp[\iota\omega(qx + s_m z - t)] \tag{46}$$

For a real-valued q, the explicit displacement formula in equation (46) simplifies to:

$$(U, \ W) = \Re(u, \ w) \approx \Re\left(\sum_{m=i}^{5} (1, \ P_m)\exp[\iota\omega(qx + s_m z - t)]\right) \tag{47}$$

The parametric form provided by equation (47) traces a closed curve representing the time-dependent trajectory and locus of a surface particle in a semiconductor medium resulting from Rayleigh wave propagation. For a specified propagation direction ($q = \cos\phi/c$ (ϕ), equation (47) demonstrates how the particle path (U, W) is influenced by the characteristics of the propagating wave. The scalar quantity $\Lambda = \sqrt{U^2 + W^2}$ denotes the maximum amplitude of particle motion (for $\widetilde{u}_m = 1$). This amplitude is directly associated with the specific generalized Rayleigh wave regime investigated in the present work.

8. Validation

- By omitting the effects of carrier density and KG nonlocality, the present thermal piezoelectric framework reduces to the limiting scenario previously analyzed by Barak and Gupta (2023). Moreover, disregarding fractional derivative terms recovers a special case corresponding to the model proposed by Ahmed *et al.* (2020).
- Additionally, by assigning the $\xi \to 0$, $\tau \to 0$ and restricting the formulation to a one-dimensional setting without fractional derivatives, the present model reduces precisely to the results obtained by Khamis *et al.* (2021).
- Furthermore, when the piezoelectric coupling is omitted and the analysis is confined to one dimension, the present model coincides with the particular case discussed by Lotfy and Sarkar (2017). This agreement arises specifically in situations where the conductive and thermal temperatures are equivalent.

9. Algorithmic procedure of solution

The analytical and numerical implementation of the proposed wave propagation model is carried out through the following sequential steps:

Step 1: The governing equations are first formulated by including Klein–Gordon-type nonlocal elasticity, fractional TPL heat conduction and semiconductor plasma effects.

Step 2: Harmonic plane wave forms are then assumed for displacement, temperature, electric potential, and carrier density.

Step 3: These wave expressions are substituted into the coupled field equations, which reduces them to a set of homogeneous algebraic equations.

Step 4: The equations are arranged in matrix form, and the determinant condition is applied for nontrivial solutions.

Step 5: This process leads to the dispersion equation governing Rayleigh-type surface wave propagation.

Step 6: The characteristic equation is solved numerically using the Durand–Kerner method while satisfying the radiation conditions.

Step 7: Phase velocity and attenuation are calculated from the resulting complex wave number.

Step 8: Finally, parametric simulations are performed to study the effects of nonlocality, fractional-order, and thermal lag parameters.

10. Numerical results and discussion

Following the theoretical formulation, this section examines the propagation behavior of generalized Rayleigh-type surface waves in a piezo-thermo-electric semiconductor medium. The governing equations are mathematically involved, making physical interpretation difficult in purely analytical form. To provide clearer insight, a numerical case study is presented to show how different heat-conduction models influence wave propagation.

Cadmium Selenide (CdSe) is selected due to its well-documented thermo-piezoelectric and semiconducting properties reported in the literature (Gupta and Barak, 2023a, 2023b; Lotfy *et al.*, 2021). The material parameters used in the present analysis are listed in Table 1. Experimental advances in semiconductor characterization now allow observation of such coupled wave phenomena. In particular, CdSe has been widely used in surface acoustic wave devices and optoelectronic sensing systems, making it suitable for experimental validation (Auld, 1973).

One possible experimental approach is laser ultrasonics (Rose, 2014), where short laser pulses generate thermoelastic surface waves and a probe beam measures the resulting displacement. This noncontact method is effective for evaluating Rayleigh wave velocity and attenuation in semiconductor media. Another technique is the pump–probe photothermal method, in which modulated thermal excitation produces coupled thermo-mechanical waves that can be monitored to study dispersion and damping. Surface acoustic wave (SAW) systems also offer a practical validation platform. By fabricating interdigital transducers on CdSe substrates, high-frequency Rayleigh waves can be generated and experimentally measured for phase velocity and attenuation. Such configurations are widely used in piezoelectric semiconductor sensing applications.

A key strength of the proposed heat-transfer framework is its ability to include higher-order fractional effects through the parameters n, p and l, which allows flexibility in tuning the model response. Earlier work by Chiriță *et al.* (2017) showed that choosing or can lead to system instability, making such cases physically unrealistic. Zampoli (2019) further reported that thermodynamic admissibility is maintained when the expansion order does not exceed four, provided suitable phase-lag parameters are considered. Based on these observations, we adopt the parameter set $\alpha = 0.9$, $n = 2$, $p = 1$, $l = 1$, $\phi = 60^0$, $\xi = 0.001$, $\tau = 0.005s$ with phase lags $\tau_q = 0.03s$, $\tau_T = 0.02s$, $\tau_v = 0.01s$. These selections ensure stability and thermodynamic consistency in line with the criteria discussed by Quintanilla and Racke (2008).

10.1 Influence of spatial nonlocal parameter on wave dispersion and damping

This subsection examines how the spatial nonlocal parameter ξ affects the propagation of Rayleigh-type surface waves within the higher-order TPL heat-conduction framework. Figure 2(a) and 2(b), present the variation of phase velocity and attenuation over a range of

Table 1. Values of key model parameters

Symbol	Value	Symbol	Value
c_{11}	$74.1\times10^{9}Nm^{-2}$	c_{33}	$83.6\times10^{9}Nm^{-2}$
c_{13}	$39.3\times10^{9}Nm^{-2}$	θ_0	$298K$
δ_1^N	$-9\times10^{-31}m^3$	τ^*	$5\times10^{-5}s$
η_{31}	$-0.160Cm^{-2}$	τ_3	$-2.9\times10^{-6}Cm^{-2}K^{-1}$
c_{55}	$13.2\times10^{9}Nm^{-2}$	$K_1^*,\ K_3^*$	$7Wm^{-1}K^{-1}s^{-1}$
β_1^T	$6.21\times10^{5}Nm^{-2}K^{-1}$	β_3^T	$5.51\times10^{5}Nm^{-2}K^{-1}$
D_1^E, D_3^E	$2.5\times10^{3}m^2/s$	η_{33}	$0.347Cm^{-2}$
ε_{33}	$9.03\times10^{-11}C^2N^{-1}m^{-2}$	η_{15}	$-0.138Cm^{-2}$
K_1, K_3	$9Wm^{-1}K^{-1}$	E_g	1.11eV
ρ	$5504\ kgm^{-3}$	C_E	$260Jkg^{-1}K^{-1}$
δ_3^N	$-7\times10^{-31}m^3$	ε_{11}	$8.26\times10^{-11}C^2N^{-1}m^{-2}$

Source(s): Created by the authors

angular frequencies. The curve $\xi = 0$ for represents the local reference case, where nonlocal effects are absent.

Figure 2(a) shows the change in phase velocity with increasing frequency. In the local case ($\xi = 0$), the velocity increases slowly and remains relatively low. When nonlocality is introduced, even at a small value such as $\xi = 0.001$, the wave speed increases noticeably. Higher values of ξ (0.002 and 0.003) shift the curves further upward, indicating faster wave propagation. This trend reflects the role of nonlocal interactions in spreading mechanical and thermal effects over a wider region. As a result, the medium responds more actively at higher frequencies, leading to increased surface wave speed compared to the local case.

Figure 2(b) presents the attenuation coefficient for the same parameter set. The local case again shows the smallest response and remains close to zero across most of the frequency range. As ξ increases, attenuation rises steadily, with the curve $\xi = 0.003$ for showing the highest growth. This indicates that nonlocal effects not only increase wave speed but also strengthen energy dissipation linked to piezo-thermo-electric coupling. Higher values of ξ make the medium more sensitive to high-frequency thermal and mechanical disturbances, resulting in greater attenuation.

Overall, Figure 2(a) and 2(b), demonstrate that spatial nonlocality strongly influences both dispersion and damping of Rayleigh-type waves. Increased nonlocal interaction accelerates propagation while simultaneously enhancing attenuation, highlighting the dual role of microstructural effects in thermo-piezoelectric semiconductor media.

10.2 Influence of temporal nonlocal parameter on wave dispersion and damping

This subsection studies the influence of the temporal nonlocal parameter τ on the propagation of Rayleigh-type waves in a thermo-piezoelectric medium under the higher-order TPL framework. Figure 3(a) and 3(b), present the variation of phase velocity and attenuation with angular frequency. The curve $\tau = 0$ for represents the classical local-in-time case, where memory effects are absent.

Figure 3(a) shows the change in phase velocity when temporal nonlocality is introduced. In the local case ($\tau = 0$), the velocity increases smoothly with frequency but remains

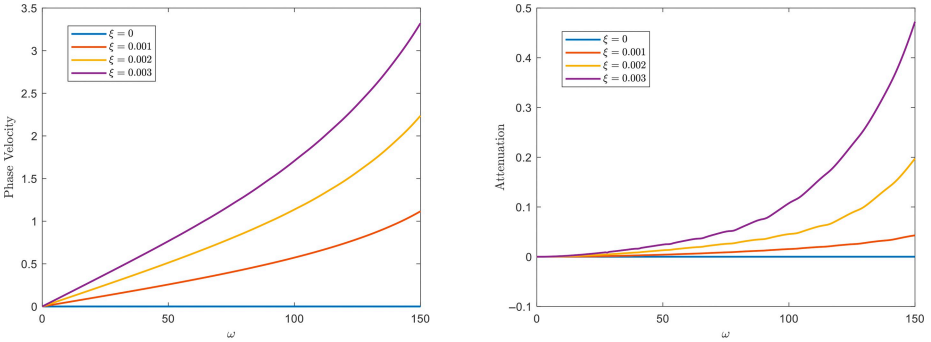

(a) **(b)**

Figure 2 (a)–(b). Variation of phase velocity and attenuation coefficient of Rayleigh-type surface waves with angular frequency (ω) for different values of the spatial nonlocal parameter ξ under the Klein–Gordon nonlocal fractional TPL heat conduction framework, while all other thermo-piezoelectric semiconductor parameters are kept fixed

Source: Created by the authors

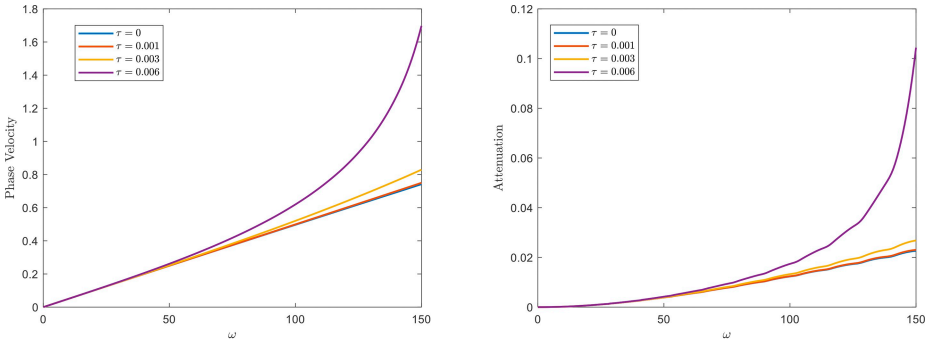

Figure 3 (a)–(b): Variation of phase velocity and attenuation coefficient of Rayleigh-type surface waves with angular frequency (ω) for different values of the temporal nonlocal parameter (τ) under the Klein–Gordon nonlocal fractional TPL heat conduction framework, while all other thermo-piezoelectric semiconductor parameters are kept fixed

Source: Created by the authors

relatively low. As τ takes small positive values (0.001, 0.003, 0.006), the curves shift upward, indicating faster wave propagation. This effect becomes stronger at higher frequencies. Temporal memory allows the medium to respond to both present and past disturbances. As a result, phase velocity increases with increasing τ. Larger reflects stronger temporal coupling within the material, enabling disturbances to travel more rapidly.

Figure 3(b) shows the variation of attenuation with the temporal nonlocal parameter τ. All curves start near zero at low frequencies, indicating a weak temporal effect in this region. As frequency increases, attenuation rises steadily. The curve $\tau = 0.006$ for shows the strongest growth. This trend suggests that temporal nonlocality enhances the energy dissipation mechanisms of the medium. As the system retains more memory of past states, thermo-mechanical interactions become stronger, leading to higher energy loss. In this sense, larger reflects stronger memory resistance to rapid fluctuations, which increases attenuation.

Overall, Figure 3(a) and 3(b), confirm that temporal nonlocality significantly affects both wave speed and damping. Stronger memory effects (τ) increase phase velocity at higher frequencies while also raising attenuation. This dual behavior highlights the combined role of temporal nonlocality within the fractional TPL thermo-piezoelectric framework.

10.3 Influence of higher-order parameter on wave dispersion and damping

This subsection examines the effect of higher-order TPL coefficients on the dispersion and damping of Rayleigh-type waves. Figure 4(a) and 4(b), depicts the evolution of phase velocity and attenuation for three distinct parameter sets: ($n = 4$, $p = 3$, $l = 3$), ($n = 3$, $p = 2$, $l = 2$) and ($n = 2$, $p = 1$, $l = 1$). These parameter sets gradually strengthen higher-order effects, allowing better representation of memory and nonlocal behavior in the medium.

Figure 4(a) displays the variation of phase velocity with angular frequency ω. The three curves show a consistent upward trend as frequency increases, but the rate of growth differs across the selected parameter sets. The combination ($n = 2$, $p = 1$, $l = 1$) yields the highest phase velocity throughout the examined range, while ($n = 4$, $p = 3$, $l = 3$) produces the lowest values, with the intermediate case ($n = 3$, $p = 2$, $l = 2$) lying between them. This ordering highlights the role of additional higher-order terms in shaping the dynamic response of the medium. As more fractional and multi-phase-lag components are introduced, the effective

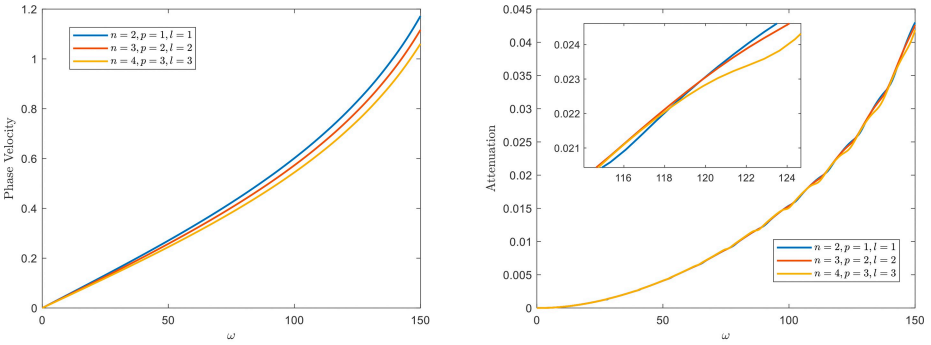

(a) **(b)**

Figure 4 (a)–(b)**:** Variation of phase velocity and attenuation coefficient of Rayleigh-type surface waves with angular frequency (ω) for different values of the higher order parameter (n, p, l) under the Klein–Gordon nonlocal fractional TPL heat conduction framework, while all other thermo-piezoelectric semiconductor parameters are kept fixed

Source(s): Created by the authors

thermal memory of the system increases. This delays the transfer of thermal and mechanical energy and slightly reduces wave speed. The inset window provides a magnified view over a narrow frequency range, showing that even small changes in higher-order coefficients cause visible shifts in phase velocity. Overall, a richer higher-order structure leads to slower but more memory-influenced wave propagation.

Figure 4(b) shows the attenuation profiles for the three higher-order models. Near $\omega = 0$, all curves almost overlap and attenuation remains negligible. This indicates that low-frequency waves are largely unaffected by the order of higher-order terms. As frequency increases, attenuation rises for all models. The inset view confirms that differences remain small in the mid-frequency range. However, beyond $\omega \approx 120$, the curves begin to separate. The model with the most advanced combination ($n = 4$, $p = 3$, $l = 3$) does not rise sharply. Instead, it gradually becomes the lowest curve within this region, while the other two remain slightly higher. This behavior suggests that adding higher-order terms does not always increase damping. In this frequency band ($n = 4$, $p = 3$, $l = 3$), the stronger hereditary structure slightly reduces attenuation, allowing more supportive wave transmission compared to lower-order cases. The separation also shows that higher-order memory effects are frequency dependent, with all models tending to converge again at very high frequencies.

This behavior indicates that, in this specific frequency band, introducing additional higher-order terms does not intensify damping. Rather, the richer hereditary structure associated with the ($n = 4$, $p = 3$, $l = 3$) model momentarily suppresses attenuation, making the medium a bit more supportive of wave transmission compared to the lower-order formulations. The subtle separation between the curves demonstrates that the influence of higher-order memory effects is frequency-dependent: they may reduce dissipation over this intermediate window even though all models converge again at very high frequencies.

10.4 Influence of fractional-order parameter on wave dispersion and damping

In this subsection, the fractional-order parameter (α) of the TPL heat-conduction model is examined to understand its impact on the phase velocity and attenuation of Rayleigh-type waves

in a thermo-piezoelectric medium with voids. Figure 5(a) and 5(b), presents the variation in these wave characteristics for four representative values of $\alpha = 0.6, 0.7, 0.8, 0.9$.

Figure 5(a) illustrates how the phase velocity responds to changes in angular frequency for several values of the fractional-order parameter α. All curves follow a nearly identical increasing trend, showing a smooth rise in velocity as the frequency increases. Although the curves almost overlap, the inset reveals a consistent and systematic separation among them. Lower values of α, such as $\alpha = 0.6$, produce slightly lower phase velocities, whereas higher values like $\alpha = 0.9$ result in marginally higher velocities across the frequency range. This gradual increase reflects the weakening of memory-driven fractional effects as α grows. When α is small, the hereditary nature of heat conduction is stronger, which slows thermo-mechanical energy transfer and reduces wave speed. As α approaches unity, the model moves closer to classical integer-order behavior, allowing disturbances to propagate more efficiently. Overall, the effect of α on dispersion remains subtle, indicating that fractional dynamics adjust the wave speed without significantly changing its overall trend.

Figure 5(b) shows the attenuation coefficient versus angular frequency for different values of the fractional-order parameter. At low frequencies, all curves almost overlap, indicating that attenuation is nearly independent of α in this region. As frequency increases, attenuation rises gradually for all cases. The inset highlights the ordering of the curves. Lower α values, which represent stronger memory effects, produce slightly higher attenuation. By contrast, larger α values correspond to lower damping. This separation becomes clearer at higher frequencies, where the curves diverge more visibly. The trend suggests that stronger fractional effects introduce additional resistance through history-dependent thermal behavior, leading to greater energy dissipation. When α increases and memory weakens, thermoelastic disturbances propagate more efficiently, reducing attenuation. Overall, attenuation shows greater sensitivity to α than phase velocity, indicating the stronger role of fractional heat conduction in wave energy loss.

The results show that the fractional-order parameter subtly influences phase velocity, but its impact on attenuation is more prominent, particularly in the high-frequency regime. Lower values of α enhance memory-driven dissipation, while higher values promote more classical (integer-order-like) behavior. This demonstrates that fractional-order effects serve

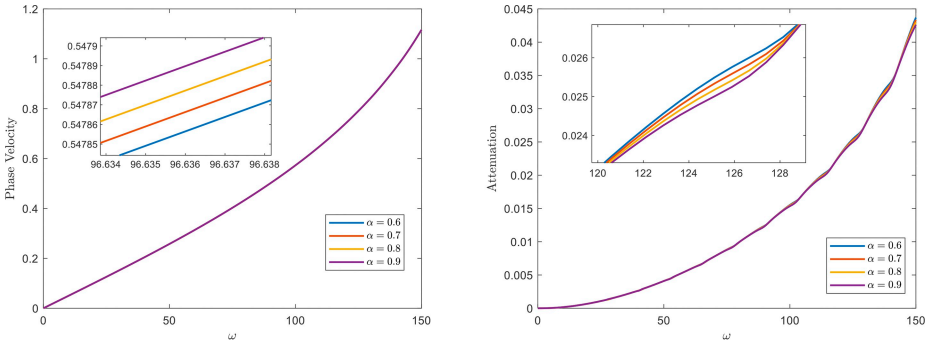

(a) **(b)**

Figure 5 (a)–(b): Variation of phase velocity and attenuation coefficient of Rayleigh-type surface waves with angular frequency (ω) for different values of the fractional order parameter (α) under the Klein–Gordon nonlocal fractional TPL heat conduction framework, while all other thermo-piezoelectric semiconductor parameters are kept fixed

Source(s): Created by the authors

as a key tunable mechanism controlling how the medium balances propagation and damping in thermo-piezoelectric environments.

10.5 Influence of distinct heat model on wave dispersion and damping

This subsection examines how different heat-conduction theories influence the phase velocity and attenuation of Rayleigh-type surface waves in a thermo-piezoelectric medium with voids. Figure 6(a) and 6(b), compares the predictions of the TPL, DPL and LS models over a broad range of angular frequencies.

Figure 6(a) displays the dependence of phase velocity on angular frequency for the three heat-conduction models. All curves show the expected monotonic increase with frequency, but each model produces a distinct magnitude of velocity. The DPL model produces the highest phase velocity throughout the full frequency range, indicating that the combined influence of two phase lags enhances the material's ability to support faster propagation of thermo-mechanical disturbances. The TPL model follows closely, lying slightly below the DPL curve but consistently above the LS model. This indicates that the additional third lag modifies the system response in a manner that keeps the velocity elevated but not to the extent observed in DPL. The LS model shows the lowest phase velocities, reflecting the more restrictive nature of classical relaxation-based heat conduction. The differences become more pronounced at higher frequencies. This indicates that adding extra lag parameters, as in the DPL and TPL models, improves the medium's ability to transmit energy under high-frequency excitation.

Figure 6(b) shows the attenuation coefficient as a function of frequency. At low frequencies, all three models behave almost identically and attenuation remains minimal. This suggests that low-frequency waves undergo very little dissipation, regardless of the heat-conduction model used. As frequency increases, attenuation rises gradually for all cases and small but consistent differences appear. The LS model remains the lowest across most of the frequency range, indicating the least energy loss. The DPL and TPL models predict slightly higher attenuation, with the TPL curve lying marginally above DPL. This behavior reflects the added dissipative contribution of phase-lag effects, which introduce extra relaxation channels in heat conduction. Unlike some earlier cases, no abrupt crossover is observed at high frequencies. All models show

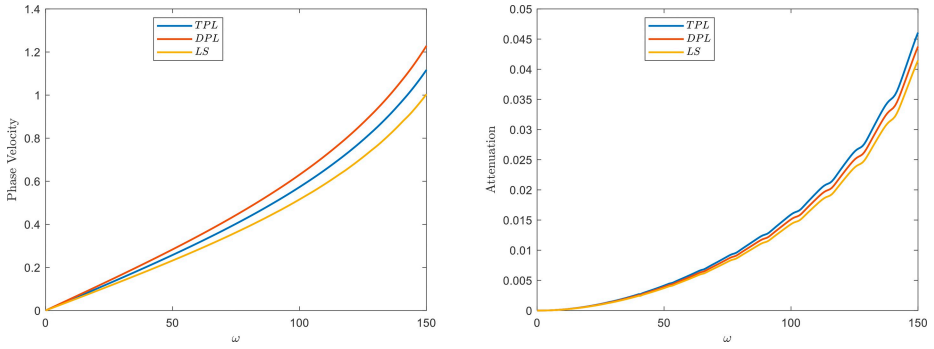

(a) **(b)**

Figure 6 (a)–(b): Variation of phase velocity and attenuation coefficient of Rayleigh-type surface waves with angular frequency (ω) for three different heat conduction model under the Klein–Gordon nonlocal fractional framework, while all other semiconductor parameters are kept fixed

Source(s): Created by the authors

comparable trends, though LS continues to remain slightly lower than DPL and TPL. Overall, the comparison shows that phase-lag-based models increase both wave speed and damping relative to the LS theory. The differences are small at low frequencies but become clearer as frequency rises, highlighting the stronger response of advanced heat-conduction models under dynamic thermal conditions.

10.6 Influence of depth on particle motion

This subsection presents the particle motion associated with Rayleigh-type waves at shallow subsurface depths under the nonlocal fractional-order TPL heat-conduction model. Figure 7(a)–7(f) illustrates the corresponding trajectories in both three-dimensional and two-dimensional views. These plots help visualize how shallow depth influences wave-induced motion. Four depth values are considered within the narrow range 1×10^{-5} to 1.1×10^{-5}, selected to capture fine variations in depth-dependent behavior.

Figure 7(a)–7(d) shows separate 3D particle trajectories for the selected depths. In each case, the motion follows the typical retrograde elliptical pattern of Rayleigh-type surface waves, combining horizontal displacement U_1 and vertical displacement U_3 over time. The overall elliptical shape remains similar across depths, but the amplitude changes noticeably. Shallower depths produce wider and more elongated loops, while slightly deeper points show more compact paths. This confirms the gradual decay of Rayleigh-wave motion with depth, consistent with classical observations (Sharma, 2023; Kumar *et al.*, 2023).

Figure 7(e) overlays all four trajectories in a single 3D plot, allowing direct comparison. The curves become progressively tighter as the depth decreases from $x_3 = 0.001$ to p $x_3 = 0.0001$, confirming that particle motion is the strongest near the free surface and diminishes steadily as the observation point moves downward. The combined plot also highlights that the rotational sense and looping rhythm remain consistent across depths the primary change lies in the shrinking amplitude envelope.

Figure 7(f) further clarifies these distinctions by projecting the trajectories onto the U_1–U_3 plane. The ellipses are clearly separated, with larger loops at shallower depths and smaller ones at deeper levels. This 2D view highlights the systematic reduction in both horizontal and vertical displacements with increasing depth.

11. Conclusions

This work investigates Rayleigh-type surface wave propagation in a piezo-thermo-electric semiconductor medium using a generalized fractional-order nonlocal TPL heat-conduction framework. The analytical and numerical results together explain how nonlocality, fractional effects, heat-conduction models and depth variations influence dispersion and damping. Based on the graphical results shown in Figures 2–7, the main findings can be summarized as follows:

- Spatial nonlocality increases phase velocity and also raises attenuation at higher frequencies, reflecting stronger microstructural interaction and energy dissipation.
- Temporal nonlocality accelerates wave propagation and introduces frequency-dependent damping, with attenuation becoming more pronounced as memory effects grow.
- Higher-order heat-conduction parameters influence both dispersion and damping. Stronger higher-order contributions increase phase velocity and enhance attenuation in the high-frequency range.
- Fractional-order effects remain subtle but systematic. Lower fractional orders slightly reduce wave speed and increase attenuation, while values closer to unity support faster propagation with lower damping.

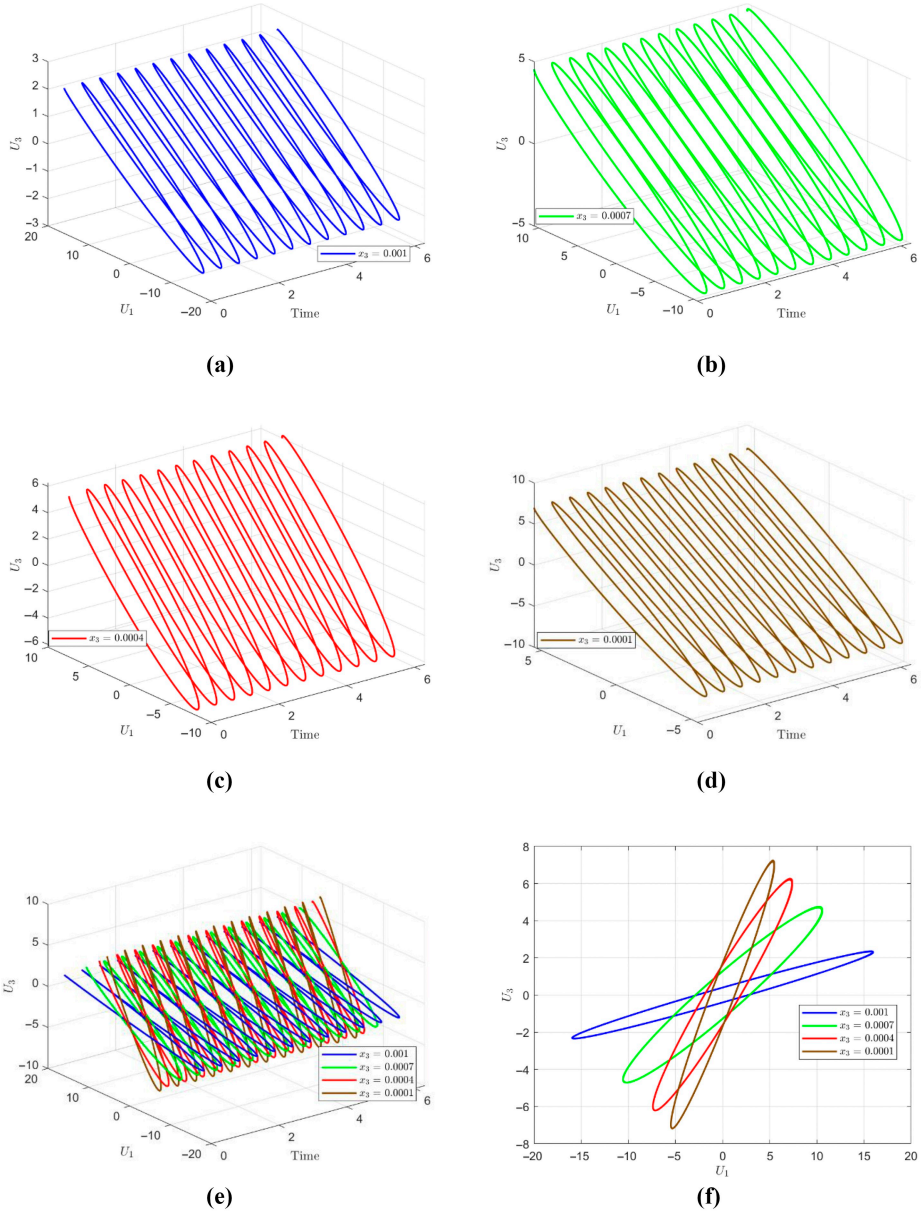

Figure 7 (a)–(f): Variation of particle motion (U, W) with time for different shallow depth Z values
Source: Created by the authors

- Comparison of heat-conduction models shows that DPL produces the highest phase velocity, followed by TPL and LS. However, LS exhibits a sharper rise in attenuation at higher frequencies due to its limited relaxation capability.
- Depth-dependent particle motion indicates larger horizontal and vertical displacements near the surface. Elliptical trajectories broaden as depth decreases, highlighting surface-localized energy concentration.

In this study, the analysis is limited to an isotropic piezo-thermo-electric semiconductor medium to focus on the combined effects of nonlocality, fractional heat conduction and plasma transport. In practice, many semiconductor crystals show strong anisotropic behavior due to their lattice structure. Extending the present model to anisotropic or functionally graded piezoelectric semiconductors would be a logical next step. Such an approach could offer deeper insight into direction-dependent wave dispersion and damping in advanced semiconductor devices.

Funding
The authors report no financial support for this research.

References

Abouelregal, A.E. (2020a), "A novel generalized thermoelasticity with higher-order time-derivatives and three-phase lags", *Multidiscipline Modeling in Materials and Structures*, Vol. 16 No. 4, pp. 689-711, doi: 10.1108/MMMS-07-2019-0138.

Abouelregal, A.E. (2020b), "Three-phase-lag thermoelastic heat conduction model with higher-order time-fractional derivatives", *Indian Journal of Physics*, Vol. 94 No. 12, pp. 1949-1963, doi: 10.1007/s12648-019-01635-z.

Abouelregal, A.E., Marin, M. and Alsharari, F. (2022), "Thermoelastic plane waves in materials with a microstructure based on micropolar thermoelasticity with two temperature and higher order time derivatives", *Mathematics*, Vol. 10 No. 9, p. 1552, doi: 10.3390/math10091552.

Abouelregal, A.E., Moustapha, M.V., Nofal, T.A., Rashid, S. and Ahmad, H. (2021a), "Generalized thermoelasticity based on higher-order memory-dependent derivative with time delay", *Results in Physics*, Vol. 20, p. 103705, doi: 10.1016/j.rinp.2020.103705.

Abouelregal, A.E., Civalek, Ö. and Oztop, H.F. (2021b), "Higher-order time-differential heat transfer model with three-phase lag including memory-dependent derivatives", *International Communications in Heat and Mass Transfer*, Vol. 128, pp. 1-12, doi: 10.1016/j.icheatmasstransfer.2021.105649.

Adel, M., Mahdy, A.M.S., El-Bary, A.A. and Lotfy, K. (2025), "Fractional and nonlocal modeling of photoacoustic plane waves in multi-temperature semiconductor media", *Rendiconti Lincei. Scienze Fisiche e Naturali*, Vol. 36 No. 3, pp. 941-958, doi: 10.1007/s12210-025-01356-y.

Agiasofitou, E. and Lazar, M. (2023), "Nonlocal elasticity of klein-gordon type with internal length and time scales: Constitutive modelling and dispersion relations", *PAMM*, Vol. 23 No. 3, p. e202300065, doi: 10.1002/pamm.202300065.

Ahmed, E.A.A., Abou-Dina, M.S. and Ghaleb, A.F. (2020), "Plane wave propagation in a piezo-thermoelastic rotating medium within the dual-phase-lag model", *Microsystem Technologies*, Vol. 26 No. 3, pp. 969-979, doi: 10.1007/s00542-019-04567-0.

Ailawalia, P., Kamel, A., Mahdy, A.M.S., Elidy, E.S. and Lotfy, K. (2025), "Thermal shock analysis in a semiconducting medium using a modified green–lindsay thermoelastic model", *Mechanics of Solids*, Vol. 60 No. 5, pp. 4050-4064, doi: 10.1134/S0025654425602861.

Anh, V. and Vinh, P. (2023), "Expressions of nonlocal quantities and application to stoneley waves in weakly nonlocal orthotropic elastic half-spaces", *Mathematics and Mechanics of Solids*, Vol. 28 No. 11, pp. 2420-2435, doi: 10.1177/10812865231164332.

Anh, V.T.N., Vinh, P.C., Tuan, T.T. and Hue, L.T. (2023), "Weakly nonlocal rayleigh waves with impedance boundary conditions", *Continuum Mechanics and Thermodynamics*, Vol. 35 No. 5, pp. 2081-2094, doi: 10.1007/s00161-023-01235-7.

Aouadi, M. (2006), "Generalized thermo-piezoelectric problems with temperature-dependent properties", *International Journal of Solids and Structures*, Vol. 43 No. 21, pp. 6347-6358, doi: 10.1016/j.ijsolstr.2005.09.003.

Auld, B.A. (1973), *Acoustic Fields and Waves in Solids*, Ripol Classic.

Barak, M.S. and Gupta, V. (2023), "Memory-dependent and fractional order analysis of the initially stressed piezo-thermoelastic medium", *Mechanics of Advanced Materials and Structures*, Vol. 31 No. 20, pp. 1-15, doi: 10.1080/15376494.2023.2211065.

Barak, M.S., Kumar, R., Kumar, R. and Gupta, V. (2023), "The effect of memory and stiffness on energy ratios at the interface of distinct media", *Multidiscipline Modeling in Materials and Structures*, Vol. 19 No. 3, pp. 464-492, doi: 10.1108/MMMS-10-2022-0209.

Biot, M.A. (1956), "Thermoelasticity and irreversible thermodynamics", *Journal of Applied Physics*, Vol. 27 No. 3, pp. 240-253, doi: 10.1063/1.1722351.

Biswas, S. (2020), "Rayleigh waves in a nonlocal thermoelastic layer lying over a nonlocal thermoelastic half-space", *Acta Mechanica*, Vol. 231 No. 10, pp. 4129-4144, doi: 10.1007/s00707-020-02751-2.

Burden, R.L., Faires, J.D. and Burden, A.M. (2015),. *Numerical Analysis*, no. 1. Cengae learning,

Chandrasekharaiah, D.S. (1988), "A generalized linear thermoelasticity theory for piezoelectric media", *Acta Mechanica*, Vol. 71 Nos 1-4, pp. 39-49, doi: 10.1007/BF01173936.

Chandrasekharaiah, D.S. (1998), "Hyperbolic thermoelasticity: a review of recent literature", *Applied Mechanics Reviews*, Vol. 51 No. 12, pp. 705-729, doi: 10.1115/1.3098984.

Chandrasekharaiah, D.S. (1986), "Thermoelasticity with second sound: a review", *Applied Mechanics Reviews*, Vol. 39 No. 3, pp. 355-376, doi: 10.1115/1.3143705.

Chen, B., Luo, C., Xia, L., Xu, L., Yan, G., Qiu, F. and Gou, G. (2024), "Research on the measurement technology for pretension stress on Small-Sized bolts based on the piezoelectric ultrasonic resonance method", *Materials*, Vol. 17 No. 23, p. 5802, doi: 10.3390/ma17235802.

Chiriță, S., Ciarletta, M. and Tibullo, V. (2017), "On the thermomechanical consistency of the time differential dual-phase-lag models of heat conduction", *International Journal of Heat and Mass Transfer*, Vol. 114, pp. 277-285, doi: 10.1016/j.ijheatmasstransfer.2017.06.071.

Choudhuri, S.R. (2007), "On a thermoelastic three-phase-lag model", *Journal of Thermal Stresses*, Vol. 30 No. 3, pp. 231-238.

de Oliveira, E.C. and Tenreiro Machado, J.A. (2014), "A review of definitions for fractional derivatives and integral", *Mathematical Problems in Engineering*, Vol. 2014 No. 1, pp. 1-6, doi: 10.1155/2014/238459.

Diethelm, K. and Ford, N.J. (2002), "Analysis of fractional differential equations", *Journal of Mathematical Analysis and Applications*, Vol. 265 No. 2, pp. 229-248, doi: 10.1006/jmaa.2000.7194.

Edelen, D.G.B. and Laws, N. (1971), "On the thermodynamics of systems with nonlocality", *Archive for Rational Mechanics and Analysis*, Vol. 43 No. 1, pp. 24-35, doi: 10.1007/BF00251543.

Eringen, A.C. (1983), "On differential equations of nonlocal elasticity and solutions of screw dislocation and surface waves", *Journal of Applied Physics*, Vol. 54 No. 9, pp. 4703-4710, doi: 10.1063/1.332803.

Eringen, A.C. and Edelen, D.G.B. (1972), "On nonlocal elasticity", *International Journal of Engineering Science*, Vol. 10 No. 3, pp. 233-248, doi: 10.1016/0020-7225(72)90039-0.

Garrappa, R. (2015), "Numerical evaluation of two and three parameter mittag-leffler functions", *SIAM Journal on Numerical Analysis*, Vol. 53 No. 3, pp. 1350-1369, doi: 10.1137/140971191.

Gorenflo, R., Mainardi, F. and Rogosin, S. (2019), "Mittag-leffler function: properties and applications", *Handbook of Fractional Calculus with Applications*, Vol. 1, pp. 269-296. doi: 10.1515/9783110571622.

Green, A.E. and Lindsay, K.A. (1972), "Thermoelasticity", *Journal of Elasticity*, Vol. 2 No. 1, pp. 1-7, doi: 10.1007/BF00045689.

Green, A.E. and Naghdi, P.M. (1991), "A re-examination of the basic postulates of thermomechanics", *Proceedings of the Royal Society of London. Series A: Mathematical and Physical Sciences*, Vol. 432 No. 1885, pp. 171-194, doi: 10.1098/rspa.1991.0012.

Green, A.E. and Naghdi, P.M. (1992), "On undamped heat waves in an elastic solid", *Journal of Thermal Stresses*, Vol. 15 No. 2, pp. 253-264.

Green, A.E. and Naghdi, P.M. (1993), "Thermoelasticity without energy dissipation", *Journal of Elasticity*, Vol. 31 No. 3, pp. 189-208, doi: 10.1007/BF00044969.

Gupta, V. and Barak, M.S. (2023a), "Fractional and MDD analysis of piezo-photo-thermo-elastic waves in semiconductor medium", *Mechanics of Advanced Materials and Structures*, Vol. 31 No. 25, pp. 1-16, doi: 10.1080/15376494.2023.2238201.

Gupta, V. and Barak, M.S. (2023b), "Quasi-P wave through orthotropic piezo-thermoelastic materials subject to higher order fractional and memory-dependent derivatives", *Mechanics of Advanced Materials and Structures*, Vol. 31 No. 22, pp. 1-15, doi: 10.1080/15376494.2023.2217420.

Gupta, V., Barak, M.S. and Das, S. (2024), "Impact of memory-dependent heat transfer on rayleigh waves propagation in nonlocal piezo-thermo-elastic medium with voids", *International Journal of Numerical Methods for Heat and Fluid Flow*, Vol. 34 No. 4, pp. 1902-1926, doi: 10.1108/HFF-10-2023-0615.

Gupta, V., Kumar, R., Kumar, M., Pathania, V. and Barak, M.S. (2023), "Reflection/transmission of plane waves at the interface of an ideal fluid and nonlocal piezothermoelastic medium", *International Journal of Numerical Methods for Heat and Fluid Flow*, Vol. 33 No. 2, pp. 912-937, doi: 10.1108/HFF-04-2022-0259.

He, Y., Yuan, M., Li, Q., Tang, L., Yang, W., Ping, Y., He, H. and Deng, B. (2025), "Feasibility study of mechanical stress wave detection in power semiconductor devices using bare FBG sensors", *IEEE Sensors Journal*, Vol. 25 No. 21, pp. 39849-39857, doi: 10.1109/JSEN.2025.3615108.

Iovane, G. and Nasedkin, A.V. (2010), "Modal analysis of piezoelectric bodies with voids. II. Finite element simulation", *Applied Mathematical Modelling*, Vol. 34 No. 1, pp. 47-59, doi: 10.1016/j.apm.2009.03.027.

Kaplunov, J., Prikazchikov, D.A. and Prikazchikova, L. (2023), "On integral and differential formulations in nonlocal elasticity", *European Journal of Mechanics - A/Solids*, Vol. 100, p. 104497, doi: 10.1016/j.euromechsol.2021.104497.

Kaplunov, J., Prikazchikov, D.A. and Prikazchikova, L. (2022), "On non-locally elastic rayleigh wave", *Philosophical Transactions of the Royal Society A: Mathematical, Physical and Engineering Sciences*, Vol. 380 No. 2231, doi: 10.1098/rsta.2021.0387.

Khamis, A.K., Lotfy, K., El-Bary, A.A., Mahdy, A.M.S. and Ahmed, M.H. (2021), "Thermal-piezoelectric problem of a semiconductor medium during photo-thermal excitation", *Waves in Random and Complex Media*, Vol. 31 No. 6, pp. 2499-2513, doi: 10.1080/17455030.2020.1757784.

Kumar, M., Kaswan, P., Sarkar, N., Liu, X. and Kumari, M. (2023), "Rayleigh waves in nonlocal generalized thermoelastic media", *International Journal of Numerical Methods for Heat and Fluid Flow*, Vol. 33 No. 6, pp. 2049-2072, doi: 10.1108/HFF-08-2022-0468.

Lazar, M. and Agiasofitou, E. (2022), "Nonlocal elasticity of klein–gordon type: fundamentals and wave propagation", *Wave Motion*, Vol. 114, p. 103038, doi: 10.1016/j.wavemoti.2022.103038.

Lewis, R.W. and Garner, R.W. (1972), "A finite element solution of coupled electrokinetic and hydrodynamic flow in porous media", *International Journal for Numerical Methods in Engineering*, Vol. 5 No. 1, pp. 41-55, doi: 10.1002/nme.1620050105.

Lewis, R.W., Huang, H.C., Usmani, A.S. and Cross, J.T. (1991), "Finite element analysis of heat transfer and flow problems using adaptive remeshing including application to solidification problems", *International Journal for Numerical Methods in Engineering*, Vol. 32 No. 4, pp. 767-781.

Lewis, R.W., Nithiarasu, P. and Seetharamu, K.N. (2004),. *Fundamentals of the Finite Element Method for Heat and Fluid Flow*, John Wiley and Sons, doi: 10.1002/0470014164.

Lewis, R.W., Navti, S.E. and Taylor, C. (1997), "A mixed lagrangian-eulerian approach to modelling fluid flow during mould filling", *International Journal for Numerical Methods in Fluids*, Vol. 25 No. 8, pp. 931-952, doi: 10.1002/(SICI)1097-0363(19971030)25:8<931::AID-FLD594>3.0.CO;2-1.

Lord, H.W. and Shulman, Y. (1967), "A generalized dynamical theory of thermoelasticity", *Journal of the Mechanics and Physics of Solids*, Vol. 15 No. 5, pp. 299-309, doi: 10.1016/0022-5096(67)90024-5.

Lotfy, K. and Sarkar, N. (2017), "Memory-dependent derivatives for photothermal semiconducting medium in generalized thermoelasticity with two-temperature", *Mechanics of Time-Dependent Materials*, Vol. 21 No. 4, pp. 519-534, doi: 10.1007/s11043-017-9340-5.

Lotfy, K., Elidy, E.S. and Tantawi, R.S. (2021), "Piezo-photo-thermoelasticity transport process for hyperbolic two-temperature theory of semiconductor material", *International Journal of Modern Physics C*, Vol. 32 No. 7, p. 2150088, doi: 10.1142/S0129183121500881.

Lotfy, K., El-Bary, A.A. and El-Sharif, A.H. (2020), "Ramp-type heating microtemperature for a rotator semiconducting material during photo-excited processes with magnetic field", *Results in Physics*, Vol. 19, p. 103338, doi: 10.1016/j.rinp.2020.103338.

Lotfy, K. and El-Bary, A.A. (2022), "Magneto-photo-thermo-microstretch semiconductor elastic medium due to photothermal transport process", *Silicon*, Vol. 14 No. 9, pp. 4809-4821, doi: 10.1007/s12633-021-01205-1.

Lotfy, K., Elidy, E.S. and Tantawi, R.S. (2021), "Photothermal excitation process during hyperbolic two-temperature theory for magneto-thermo-elastic semiconducting medium", *Silicon*, Vol. 13 No. 7, pp. 2275-2288, doi: 10.1007/s12633-020-00795-6.

Mahdy, A.M.S., Abdou, M.A. and Mohamed, D.S. (2026), "Stability and numerical solution for solving nonlinear fractional integro-differential equations with phase lag", *Journal of Applied Mathematics and Computing*, Vol. 72 No. 1, p. 28, doi: 10.1007/s12190-025-02655-1.

Mindlin, R.D. (1974), "Equations of high frequency vibrations of thermopiezoelectric crystal plates", *International Journal of Solids and Structures*, Vol. 10 No. 6, pp. 625-637, doi: 10.1016/0020-7683(74)90047-X.

Neamen, D. (1992), *Semiconductor Physics and Devices Basic Principles*, Tata McGraw Hill Education.

Pathania, V., Kumar, R., Gupta, V. and Barak, M.S. (2023), "Double porous thermoelastic waves in a homogeneous, isotropic solid with inviscid liquid", *Archive of Applied Mechanics*, Vol. 93 No. 5, pp. 1943-1962, doi: 10.1007/s00419-023-02364-w.

Pathania, V., Kumar, R., Gupta, V. and Barak, M.S. (2022), "Generalized plane waves in a rotating thermoelastic double porous solid", *International Journal of Applied Mechanics and Engineering*, Vol. 27 No. 4, pp. 138-154, doi: 10.2478/ijame-2022-0055.

Quintanilla, R. and Racke, R. (2008), "A note on stability in three-phase-lag heat conduction", *International Journal of Heat and Mass Transfer*, Vol. 51 Nos 1-2, pp. 24-29, doi: 10.1016/j.ijheatmasstransfer.2007.04.045.

Romano, G., Barretta, R., Diaco, M. and Marotti de Sciarra, F. (2017), "Constitutive boundary conditions and paradoxes in nonlocal elastic nanobeams", *International Journal of Mechanical Sciences*, Vol. 121, pp. 151-156, doi: 10.1016/j.ijmecsci.2016.10.036.

Rose, J.L. (2014), *Ultrasonic Guided Waves in Solid Media*, Cambridge University Press, doi: 10.1017/CBO9781107273610.

Saeed, T. and Abbas, I. (2022), "Effects of the nonlocal thermoelastic model in a thermoelastic nanoscale material", *Mathematics*, Vol. 10 No. 2, pp. 1-10, doi: 10.3390/math10020284.

Sharma, M.D. (2023), "Propagation of generalised rayleigh wave at the surface of piezoelectric medium with arbitrary anisotropy", *ZAMM Zeitschrift Fur Angewandte Mathematik Und Mechanik*, Vol. 103 No. 3, pp. 1-15, doi: 10.1002/zamm.202000160.

Smith, R.C. (2005), *Smart Material Systems*, Society for Industrial and Applied Mathematics, Philadelphia, doi: 10.1137/1.9780898717471.

Tzou, D.Y. (1995), "A unified field approach for heat conduction from macro- to micro-scales", *Journal of Heat Transfer*, Vol. 117 No. 1, pp. 8-16, doi: 10.1115/1.2822329.

Wang, J.L. and Li, H.F. (2021), "Memory-dependent derivative versus fractional derivative (I): difference in temporal modeling", *Journal of Computational and Applied Mathematics*, Vol. 384, p. 112923, doi: 10.1016/j.cam.2020.112923.

Yadav, A.K., Carrera, E., Marin, M. and Othman, M.I.A. (2022), "Reflection of hygrothermal waves in a nonlocal theory of coupled thermo-elasticity", *Mechanics of Advanced Materials and Structures*, Vol. 31 No. 5, pp. 1-14, doi: 10.1080/15376494.2022.2130484.

Zampoli, V. (2019), "On the increase in signal depth due to high-order effects in micro-and nanosized deformable conductors", *Math. Probl. Eng*, Vol. 2019, pp. 1-11, doi: 10.1155/2019/2629012.

Zhang, L.L., Liu, J.X., Fang, X.Q. and Nie, G.Q. (2014), "Effects of surface piezoelectricity and nonlocal scale on wave propagation in piezoelectric nanoplates", *European Journal of Mechanics - A/Solids*, Vol. 46, pp. 22-29, doi: 10.1016/j.euromechsol.2014.01.005.

Corresponding author
Vipin Gupta can be contacted at: vipin@gurugramuniversity.ac.in